Atmos. Chem. Phys. Discuss., 6, 12301–12345, 2006
www.atmos-chem-phys-discuss.net/6/12301/2006/

Atmospheric Chemistry and Physics Discussions

Near-real time retrieval of tropospheric NO_2 from OMI

K. F. Boersma[1,*], H. J. Eskes[1], J. P. Veefkind[1], E. J. Brinksma[1], R. J. van der A[1], M. Sneep[1], G. H. J. van den Oord[1], P. F. Levelt[1], P. Stammes[1], J. F. Gleason[2], and E. J. Bucsela[2]

[1]KNMI, De Bilt, The Netherlands
[2]NASA GSFC, Greenbelt, Maryland, USA
[*]now at: Harvard University, Cambridge, USA

Received: 7 November 2006 – Accepted: 17 November 2006 – Published: 29 November 2006

Correspondence to: K. F. Boersma (boersma@fas.harvard.edu)

Abstract

We present a new algorithm for the near-real time retrieval – within 3 h of the actual satellite measurement – of tropospheric NO_2 columns from the Ozone Monitoring Instrument (OMI). The retrieval system is based on the combined retrieval-assimilation-modelling approach developed at KNMI for off-line tropospheric NO_2 from the GOME and SCIAMACHY satellite instruments. We have adapted the off-line system such that the required a priori information – profile shapes and stratospheric background NO_2 – is now immediately available upon arrival of the OMI NO_2 slant columns and cloud data at KNMI. Slant column NO_2 and cloud information arrives at KNMI typically within 80 min of actual OMI observations. Slant columns for NO_2 are retrieved using differential optical absorption spectroscopy (DOAS) in the 405–465 nm range. Cloud fraction and cloud pressure are provided by a new cloud retrieval algorithm that uses the absorption of the O_2–O_2 collision complex near 477 nm. On-line availability of stratospheric slant columns and NO_2 profiles is achieved by running the TM4 chemistry transport model (CTM) forward in time based on forecast ECMWF meteo and assimilated NO_2 information from all previously observed orbits. OMI NO_2 slant columns, after correction for spurious across-track variability, show a random error for individual pixels of approximately 0.7×10^{15} molec.cm^{-2}. As NO_2 retrievals are very sensitive to clouds, we evaluated the consistency of cloud fraction and cloud pressure from the new O_2–O_2 (OMI) algorithm and from the Fast Retrieval Scheme for Cloud Observables (FRESCO). Cloud parameters from the O_2–O_2 (OMI) algorithm have similar frequency distributions as cloud parameters retrieved from FRESCO (SCIAMACHY) for August 2006. On average, OMI cloud fractions are higher by 0.011, and OMI cloud pressures exceed FRESCO cloud pressures by 60 hPa. As a consistency check, we intercompared OMI near-real time NO_2 columns measured at 13:45 h local time to SCIAMACHY off-line NO_2 columns measured at 10:00 h local time. In August 2006, both instruments observe very similar spatial patterns of tropospheric NO_2 columns, and small differences for most locations on Earth where tropospheric NO_2 columns

are small. For regions that are strongly polluted, SCIAMACHY observes higher tropospheric NO_2 columns than OMI.

1 Introduction

The daily global coverage and the pixel size of $24 \times 13\,km^2$ make the Ozone Monitoring Instrument (OMI) on the Earth Observing System (EOS) Aura satellite well suited to observe the sources of air pollution with an unprecedented spatial and temporal coverage. Recently, satellite-based observations of tropospheric NO_2 have been proven useful in estimating anthropogenic emissions of nitrogen oxides (Leue et al., 2001; Martin et al., 2003, 2006; Beirle et al., 2003; Richter et al., 2005; van der A et al., 2006), in observing emissions by soils (Jaeglé et al., 2004), and in putting constraints on NO_x production by lightning (Beirle et al., 2004, 2005; Boersma et al., 2005). Tropospheric NO_2 columns derived from the Global Ozone Monitoring Experiment (GOME) have been compared with outputs from various-scale models (Velders et al., 2001; Lauer et al., 2002; Savage et al., 2004; Ma et al., 2006). The results of the regional-scale chemistry-transport model CHIMERE have been evaluated against GOME and SCIAMACHY-derived tropospheric NO_2 columns (Konovalov et al., 2004; Blond et al., 2006[1]). These comparisons have clearly demonstrated the potential of satellite NO_2 data sets for model evaluation and emission estimates. On the other hand, sometimes large and often systematic differences persist between retrievals by different groups (van Noije et al., 2006), calling into question the quality of space-based constraints on NO_x sources. However, validation efforts for various retrievals show acceptable accuracy (Heland et al., 2002; Petritoli et al., 2004; Martin et al., 2004, 2006; Cede et al., 2006; Ordóñez et al., 2006; Schaub et al., 2006) for GOME and SCIAMACHY NO_2.

[1] Blond, N., Boersma, K. F., Eskes, H. J., van der A, R., Van Roozendael, J. M., De Smedt, I., Bergametti, G., and Vautard, R.: Intercomparison of SCIAMACHY nitrogen dioxide observations, in-situ measurements and air quality modeling results over Western Europe, submitted, J. Geophys. Res., 2006.

The unique characteristics of OMI -the small pixel size and daily global coverage– allow for an important contribution to air quality monitoring and modelling. GOME has a resolution of 320×40 km^2, too coarse to resolve the areas with high emissions that are relevant in regional air quality modelling, e.g. medium-sized cities. SCIAMACHY's horizontal resolution is 60×30 km^2 but needs six days to achieve global coverage. Despite the fact that interesting regional-scale daily variability has been observed with SCIAMACHY by Blond et al. (2006)[1], it is not well suited for a day-to-day monitoring of air quality. The daily coverage of OMI has been an important motivation to set up the near-real time NO_2 retrieval system described in this paper. An additional motivation originates from the data set of tropospheric NO_2 columns retrieved from the GOME and SCIAMACHY instruments that now spans more than 10 years (1996–2006) and is publicly available through http://www.temis.nl. NO_2 data sets from GOME and SCIAMACHY have been retrieved with one and the same retrieval-assimilation-modelling approach described in Boersma et al. (2004) and show excellent mutual consistency (van der A et al., 2006). The OMI NO_2-retrievals described here are expected to add considerable value to the GOME and SCIAMACHY dataset. Health regulations concerning air quality require a routine monitoring, typically on an hourly basis, of surface concentrations of several species including NO_2. Clearly, this requirement cannot be directly fulfilled by satellite instruments in general, nor by OMI in particular. Nevertheless we anticipate that instruments like OMI will make essential contributions to air quality monitoring and modelling:

- Daily maps of NO_2 columns provided by OMI show extensive transport features that are changing from day to day, and that are politically interesting as they directly show air pollution being transported across national borders. These changeable distributions can be directly compared with model output, and they constitute strong tests for the description of horizontal and vertical transport processes, as well as NO_x removal processes.

- A direct relationship exists between columns of NO_2 and surface emissions of

NO_x. OMI data can thus be combined with regional-scale models through inverse modeling or data assimilation to adjust or improve emission estimates in the model and to detect unknown sources.

- Incidental releases, such as from major fires, can be monitored and quantified, and subsequent plumes can be tracked from day to day.
- A routine assimilation of satellite data may improve air quality "nowcasting" and forecasting capabilities, and may thereby contribute to the monitoring of emission and health regulations.

All these applications are new and largely untested. Despite this, there exists a considerable interest in the community to establish atmospheric chemistry data assimilation systems that will exploit the available satellite data sets of atmospheric composition and air pollution. One example is the European GEMS project (Global and regional Earth-system (Atmosphere) Monitoring using Satellite and in-situ data; (http://www.ecmwf.int/research/EU/projects/GEMS/) which is scheduled to deliver an operational atmospheric composition assimilation system by 2009.

This paper presents a new retrieval algorithm designed for near-real time retrieval of tropospheric NO_2 from OMI. This algorithm differs from the standard, off-line OMI NO_2 retrieval-procedure that is a joint NASA/KNMI effort and has been described by Bucsela et al. (2006). The differences are shortly discussed in Sect. 3.1. In Sect. 2 we shortly discuss Ozone Monitoring Instrument characteristics, and describe the fast transport of measurement data from the satellite to the computer system where the retrievals take place. The retrieval itself is discussed in Sect. 3, with a focus on the innovations with respect to previous NO_2 column retrieval work at KNMI. Section 4 is devoted to errors in the NO_2 slant columns that occur through calibration errors in current the level 1 data, and through the propagation of measurement noise in the spectral fitting. The stratospheric correction and computation of the air mass factor (AMF) are described in Sect. 5. As SCIAMACHY and OMI cloud retrieval use different spectral features, we also discuss in Sect. 5 the consistency of the OMI O_2–O_2 cloud

product with the SCIAMACHY FRESCO cloud retrievals. As a first order quality-check of OMI near-real time NO_2 retrievals, in Sect. 6 we compare SCIAMACHY and OMI tropospheric NO_2 columns for the month August 2006 and show some examples of OMI's capabilities. This is followed by conclusions in Sect. 7.

2 OMI overview

2.1 Ozone Monitoring Instrument

The Dutch-Finnish Ozone Monitoring Instrument (OMI) on NASA's EOS Aura satellite is a nadir-viewing imaging spectrograph measuring direct and atmosphere-backscattered sunlight in the ultraviolet-visible (UV-VIS) range from 270 nm to 500 nm (Levelt et al., 2006a). EOS Aura was launched on 15 July 2004 and traces a Sun-synchronous, polar orbit at approximately 705 km altitude with a period of 100 min and a local equator crossing time between 13.40 h and 13.50 h. In contrast to its predecessors GOME and SCIAMACHY, instruments operating with scanning mirrors and one-dimensional photo diode array detectors, OMI has been equipped with two two-dimensional CCD detectors. The CCDs record the complete 270–500 nm spectrum in one direction, and observe the Earth's atmosphere with a 114° field of view, distributed over 60 discrete viewing angles, perpendicular to the flight direction. OMI's wide field of view corresponds to a 2600 km wide spatial swath on the Earth's surface for one orbit, large enough to achieve complete global coverage in one day. The exposure time of the CCD-camera measures 2 s, corresponding to a spatial sampling of 13 km along track (2 s × 6.5 km/s, the latter being the orbital velocity projected onto the Earth's surface). Across track the size of an OMI pixel varies with viewing zenith angle from 24 km in the nadir to approximately 60 km for the extreme viewing angles of 57° at the edges of the swath. OMI has three spectral channels; UV1 (270–310 nm) and UV2 (310–365 nm) are covered by CCD1. CCD2 covers the VIS-channel from 365–500 nm with a spectral sampling of 0.21 nm and a spectral resolution of 0.63 nm. It is in this channel that the

spectral features of NO_2 are most prominent. The spectral resolution and sampling of OMI have been designed to resolve trace gas absorption signatures of chemically important atmospheric species. The spectral sampling rate (resolution/sampling) is ~3, large enough to avoid spectral undersampling or aliasing difficulties in the spectral fitting process. A polarization scrambler makes the instrument insensitive to the polarization state of the reflected Earth radiance to less than 0.5%. During nominal operations OMI takes one measurement of the solar irradiance per day. Radiometric calibration is accomplished in-flight by a series of special on-board measurements that involve a.o. monitoring detector degradation with a white-light source, and dark signal measurements when OMI is at the dark side of the Earth. Spectral calibration is achieved by a cross-correlation of Fraunhofer lines in theoretical and observed in-flight irradiance spectra. For more details on the instrument and calibration procedures, the reader is referred to Dobber et al. (2005, 2006).

Retrievals of ozone column and vertical distribution (as well as BrO and OClO) are meant to address the first EOS Aura science question whether the ozone layer is recovering. Of no less importance are the retrievals of trace gases related to air pollution and the production of photochemical smog, i.e. NO_2, HCHO, and SO_2. In addition, cloud and aerosol parameters, and UV-B surface flux are derived from OMI. For an overview of EOS-AURA and OMI targets, see Levelt et al. (2006b). In this paper we focus on the fast delivery of OMI NO_2 data relevant for the purposes of air quality monitoring and forecasting.

2.2 Data transport

OMI science data is stored on-board on a solid-state recorder. These unprocessed data are down-linked once every orbit (100 min) to one of the Polar Ground Stations in Alaska or Svalsbard (Spitsbergen) or to the Wallops Ground Station in Virginia (USA). As soon as a spacecraft contact session has finished, the OMI data are sent to the EOS Data Operations System (EDOS) at NASA GSFC in Maryland (USA). At GSFC, the raw OMI data are processed in three different ways, resulting in Rate-Buffered

Data, Expedited Data, and Production Data. Near-real time processing is based on Rate-Buffered Data (RBD). RBD data are made available with the highest priority, at the expense of data integrity. The other data types are scheduled for off-line level 2 retrievals.

EDOS subsequently forwards the RBD data to the OMI Science Investigator-led Processing System (SIPS), where production starts as soon as all engineering, ancillary and science data have been received. A preprocessor run improves data integrity, removes duplicate packages, and time-orders the data. Then, the resulting level 0 data sets (in Analog to Digital Units) are processed into level 1b data, i.e. estimated radiances and irradiances in units of W/m^2/nm(/sr) (van den Oord et al., 2006). The only difference with standard production at this time is that the near-real time processing uses the predicted altitude and ephemeris data received from the spacecraft rather than definitive altitude and ephemeris data. Using predicted orbital parameters may lead to errors in geolocation parameters (latitude, longitude, solar, viewing, and azimuth angles) that influence the retrievals, but in practice, these errors are small. Once OMI level 1b data has been generated at the SIPS, the O_2–O_2 cloud level 1–2 algorithm (Acarreta et al., 2004) is run, followed by the DOAS ozone (Veefkind and De Haan, 2002) and NO_2 slant column spectral fitting retrieval algorithms. As soon as the ozone and NO_2 slant column files are available, they are picked up by the OMI Dutch Processing system (ODPS) and forwarded to the processing system at KNMI developed within the DOMINO project (see acknowledgment). Subsequent steps are intrinsic parts of the DOMINO retrieval algorithm and are described in the next section.

Typical data volumes per orbit are 450 MB level 0 data, 400 MB level 1b data, and 17 MB NO_2 slant column data (including cloud retrievals). Processed orbital data arrives at KNMI on average within three hours after the start of an orbit. An orbit takes 100 min (indicated as the red part of Fig. 1) and the process described above (downlink, transfer to EDOS, transfer to SIPS, level 1b and 2 processing, and transfer to KNMI) takes 80 min (the orange part in Fig. 1). Final processing from NO_2 slant columns to tropospheric vertical columns at KNMI is typically faster than 2 min on a linux worksta-

tion. Including the generation of images and web publishing, the processing step takes less than 45 min (the green part of Fig. 1), so that data and images are available for the public at approximately 16:00 h local time.

3 Algorithm description

3.1 Heritage: the retrieval-assimilation-modelling approach

The near-real time NO_2 retrieval algorithm (DOMINO version: TM4NO2A-OMI v0.8, February 2006) in this work is based on the retrieval-assimilation-modelling approach (hereafter: RAM) described in Boersma et al. (2004). The first DOAS slant column fitting part is identical to the standard, off-line OMI NO_2 product discussed by Bucsela et al. (2006). The RAM-approach has been applied at KNMI to generate a tropospheric NO_2 data base from GOME and SCIAMACHY measurements. The off-line RAM approach consists of a three-step procedure:

1. a slant column density is determined from a spectral fit to the Earth reflectance spectrum with the so-called DOAS approach (differential absorption spectroscopy, e.g. Platt, 1994; Boersma et al., 2002; Bucsela et al., 2006),
2. the stratospheric contribution to the slant column is estimated from assimilating slant columns into a CTM including stratospheric chemistry and wind fields, and
3. the residual tropospheric slant column is converted into a vertical column by application of a tropospheric air mass factor (AMF).

The standard, off-line NO_2 product and the near-real time retrieval have step 1 in common. This step is discussed in detail in Sects. 3.2 and 3.3. Step 2 and 3 are different between the OMI off-line and NRT algorithms, for details the reader is referred to Bucsela et al. (2006); Boersma et al. (2004) and this work.

Until now, a large NO_2 data set has been generated with the RAM-approach for the GOME and SCIAMACHY instruments. The data sets cover the period April 1996–June 2003 for GOME and from January 2003 onwards for SCIAMACHY. The two data sets contain tropospheric NO_2 columns along with error estimates and averaging kernels (Eskes and Boersma, 2003) for every individual pixel and they are publicly available through http://www.temis.nl. NO_2 retrieved from GOME with the RAM approach has been used to estimate the production of NO_x by lightning in the tropics (Boersma et al., 2005). Furthermore, Schaub et al. (2006) showed that GOME tropospheric NO_2 over Northern Switzerland in the period 1996–2003 compares favourably to NO_2 profiles observed with in-situ techniques. Blond et al. (2006)[1] reported considerable consistency between SCIAMACHY tropospheric NO_2 columns and both surface observations as well as simulations from the regional air-quality model CHIMERE over Europe, especially over moderately polluted rural areas. Merged GOME and SCIAMACHY observations showed a distinct increase in NO_2 columns from 1996 to 2003 over China, consistent with a strong growth of NO_x emissions in that area (van der A et al., 2006). Moreover, this paper showed an almost seamless continuity from GOME to SCIAMACHY NO_2 values retrieved with the same RAM-approach. This finding provides confidence in the consistency of the two data sets and their retrieval method, even though they originated from two different satellite instruments (with similar overpass times of 10:30 h (GOME) and 10:00 h (SCIAMACHY)).

Tropospheric NO_2 columns are generally retrieved as follows:

$$V_{tr} = \frac{S - S_{st}}{M_{tr}(\mathbf{x_{a,tr}}, \mathbf{b})}, \quad (1)$$

with S the slant column density from step 1, S_{st} the stratospheric slant column obtained from step 2, and M_{tr} the tropospheric AMF that depends on the a priori NO_2 profile $\mathbf{x_{a,tr}}$ and the set of forward model paramaters $\mathbf{b}$ including cloud fraction, cloud pressure, surface albedo, and viewing geometry.

For the RAM-approach as well as the NRT-retrieval described here, AMFs and averaging kernels are computed with a pseudo-spherical version of the DAK radiative

transfer model (Stammes, 2001). Given the best estimate of the forward model parameters the DAK forward model describes the scattering and absorbing processes that define the average optical path of photons from the Sun through the atmosphere to the OMI.

Also similar as in our RAM-approach for off-line retrievals, we obtain here the a priori NO_2 profile shapes ($\mathbf{x}_{a,tr}$) from the global chemistry-transport model TM4 at a resolution of 2° latitude by 3° longitude and 35 vertical levels extending up to 0.38 hPa. Given the very few available in situ NO_2 measurements, a global 3-D model of tropospheric chemistry is the best source of information for the vertical distribution of NO_2 at the time and location of the OMI measurement. The TM4 model is driven by forecast and analysed six hourly meteorological fields from the European Centre for Medium Range Weather Forecast (ECMWF) operational data. These fields include global distributions for horizontal wind, surface pressure, temperature, humidity, liquid and ice water content, cloud cover and precipitation. A mass conserving preprocessing of the meteorological input is applied according to Bregman et al. (2003). Key processes included are mass conserved tracer advection, convective tracer transport, boundary layer diffusion, photolysis, dry and wet deposition as well as tropospheric chemistry including non-methane hydrocarbons to account for chemical loss by reaction with OH (Houweling et al., 1998). In TM4, anthropogenic and natural emissions of NO_x are based on results from the EU POET-project (Precursors of Ozone and their Effects on the Troposphere) for the year 1997 (Olivier et al., 2003). Including free tropospheric emissions from air traffic (0.8 Tg N/yr) and lightning (5 Tg N/yr), total NO_x emissions for 1997 amount to 46 Tg N/yr.

As in the RAM-approach for GOME and SCIAMACHY retrievals, cloud fraction and cloud pressure are determined from the actual satellite measurements. Because OMI does not detect the O_2 A band at 760 nm, we use cloud parameters retrieved from the VIS-channel using the O_2–O_2 absorption feature at 477 nm (Acarreta et al., 2004). The cloud retrieval is based on the same set of assumptions (i.e. clouds are modelled as Lambertian reflectors with albedo 0.8) as the FRESCO-algorithm (Koelemeijer et al.,

2001). Before launch, the precision of the O_2–O_2 cloud fraction and cloud pressure was discussed in Acarreta et al. (2004) with encouraging results. In Sect. 5.2.1 we test the accuracy of the O_2–O_2 cloud parameters by comparing them to FRESCO cloud parameters retrieved by SCIAMACHY on the same days and same locations.

As for GOME and SCIAMACHY retrievals, we use a surface albedo database derived from TOMS and GOME Lambert-equivalent reflectivity (LER) measurements at 380 nm and 440 nm as described in Boersma et al. (2004). These monthly average surface albedo maps have a spatial resolution of $1^\circ \times 1.25^\circ$ and represent climatological (monthly) mean situations. The uncertainty in the surface albedo is estimated to be approximately 0.01 (Koelemeijer et al., 2003; Boersma et al., 2004).

In summary, the near-real time algorithm is based on the RAM-approach used for GOME and SCIAMACHY retrievals at KNMI. The main differences with RAM are: (1) near-real time requirement, (2) different spectral fitting method, and (3) cloud inputs derived from (similar but) different algorithms. The near-real time algorithm differs from the off-line standard NASA/KNMI NO_2 algorithm in the method to estimate the stratospheric NO_2 content, in the choice of radiative transfer model, and in the a priori NO_2 profiles and different surface albedo data sets for AMF computations

3.2 Near-real time retrieval

The most important difference between the RAM-approach and the NRT-retrieval is related to the required near-real time delivery of the retrieval product. In the RAM-approach, the estimated stratospheric NO_2 column (step 2) and the modelled profile shape (required for step 3), are provided by off-line assimilation and modelling based on analysed ECMWF meteorological data. In contrast, for the NRT-retrieval, the assimilation and modelling steps are operational, based on daily ECMWF meteorological analyses and forecasts.

The NRT-retrieval consists of two distinct subsystems. The first is the TM forecast subsystem shown in Fig. 2. This forecast system is run once per day, as soon meteorological data becomes available. The second subsystem is activated each and every

time that new OMI data becomes available, and incorporates the model information provided by subsystem 1.

In the forecast subsystem (1), the actual chemical state of the atmosphere is based on the analysis and forecast run starting from the analysis of the previous day. The update consists of running the chemistry-transport model forward in time with the forecast ECMWF meteorological data and the assimilation of all available OMI NO_2 slant columns measurements. The updated analysis, the new actual state, is then stored as input for a subsequent time step. The outputs are the necessary inputs to the near-real time subsystem (2); the stratospheric NO_2 column and the NO_2 and temperature profiles (needed in AMF computations).

The NRT-subsystem is illustrated in Fig. 2. As soon as an orbit of observed NO_2 slant columns arrives at KNMI, the forecast TM stratospheric slant column, prepared by the TM forecast subsystem, is ready and is subtracted. Subsequently, the residual tropospheric slant column is converted into a vertical column by the tropospheric AMF. The AMF is computed as described as in Sect. 3.1. The averaging kernel is also calculated for output and furthermore serves as the observation operator required in the assimilation part of the TM forecast subsystem.

3.3 Slant column retrieval

A second difference between the OMI near-real time and SCIAMACHY off-line implementation is the wide spectral window that is used in the DOAS retrieval. For GOME and SCIAMACHY, it has been conventional wisdom that a 425–450 nm window yields the most precise and stable fitting results. For OMI a much wider fit window, 405–465 nm, has been proposed by Boersma et al. (2002) in order to compensate for OMI's lower signal-to-noise ratio (approximately 1400 under normal mid-latitude conditions) compared to GOME and SCIAMACHY (approximately 2000, Bovensmann et al., 1999) in this wavelength region. Pre-flight testing showed that a least squares fitting of reference spectra from NO_2, O_3, a theoretical Ring function, and a 3rd order polynomial to the reflectance spectrum yields results that are stable for multiple viewing geometries

with a better than 10% NO_2 slant column precision (Boersma et al., 2002). The NO_2 absorption cross section spectrum is taken from Vandaele et al. (1998), who tabulated the cross section at different temperatures. To account for the temperature sensitivity of the NO_2 cross section spectrum – determined from the data by Vandaele et al. (1998) – an effective atmospheric temperature is calculated for the NO_2 along the average photon path. Subsequently an *a posteriori* correction for the difference between the computed effective temperature and the 220 K cross section spectrum used in the fitting procedure is applied (Boersma et al., 2002). The ozone absorption cross section spectrum is taken from WMO (1975) and the theoretical Ring spectrum from De Haan (personal communication, 2006) based on irradiance data by Voors et al. (2006). All reference spectra have been convolved with the OMI instrument transfer function (Dobber et al., 2005). OMI NO_2 slant column retrieval with synthetic and flight model data (Dobber et al., 2005) yields results that fulfill the OMI science requirement of better than 10% slant column precision (Boersma et al., 2002; Bucsela et al., 2006). However, upon first inspection of actual flight-data, systematic enhancements in the OMI NO_2 slant columns show up at specific satellite viewing angles. This across-track variability is has also been reported by Kurosu et al. (2005) for HCHO-retrievals. Below we discuss a procedure to reduce across-track variability and investigate the error budget of the OMI NO_2 slant columns.

4 Slant column density errors

4.1 Across-track variability

Calibration errors in the level 1b OMI irradiance measurements used here are likely responsible for across-track variability observed in the NO_2 slant columns. This variability will likely be significantly reduced in future level 1b releases with improved calibration data (expected in Spring 2007), using daily dark current corrections. Across-track variability appears as constant offsets for specific satellite viewing angles along an orbit,

allowing for an a posteriori correction that consists of four steps:

1. Determine the orbital segment (50 along track by 60 across track pixels in size) with the minimum variance in NO_2 columns.

2. Within this window, average the 50 NO_2 columns with the same viewing angle. This gives 60 average across-track NO_2 columns.

3. Separate low and high frequencies of the across-track columns with a Fourier analysis.

4. Perform the correction by subtracting the (high-frequency) across-track variability for all across-track rows along the orbit.

In this scheme, the selection of the minimum variance window avoids areas with large anthropogenic emissions. The high-frequencies are then interpreted as the across-track variability due to calibration errors in the OMI level 1b data. Similarly, the low frequencies describe any (weak, stratospheric) natural variability. The low frequencies are described by the first three Fourier terms. Subsequently we subtract the high-frequency signal obtained for the minimum variance window for all rows along the orbit. If it turns out to be not possible to determine a correction for a particular orbit, the across-track variability correction from the previous orbit is taken.

Figure 4 shows corrections for across-track variability computed from 10 consecutive orbits measured on the same day (22 September 2004). Although the corrections have been computed from independent data, they are remarkably similar. This justifies taking the correction determined from the previous orbit if for some reason a correction cannot be determined from the actual orbit. Furthermore, Fig. 4 provides further evidence that irradiance data are most likely at the basis of the across-track variability. All orbits shown have been retrieved with the same irradiance measurement. However, when the correction was plotted for the first orbit retrieved with a new irradiance measurement, a distinctly different correction pattern was seen (not shown).

ACPD
6, 12301–12345, 2006

4.2 Slant column precision

In this section we estimate the DOAS fitting error of individual NO_2 slant columns. We do so by a statistical analysis of OMI NO_2 columns observed over separate 2°×2° boxes in the meridional band between 178° and 180° W. The basic assumption is that the OMI pixels within a 2°×2° box observe the same total vertical column over this clean part of the Pacific Ocean. Any variability in the observed total vertical columns is assumed to originate from errors in the slant columns if the ensemble of AMFs within a box has little variability. Boxes with appreciable AMF variability were rejected if the box-mean vertical column computed by averaging the ensemble of individual slant columns ratioed by a box-mean AMF ($\overline{V'}$) differed by more than 0.1% with the box-mean vertical column computed by averaging the ensemble of individual slant columns ratioed by the original AMFs ($\overline{V}$). We find that for most of the 2°×2° boxes, $\overline{V}$ and $\overline{V'}$indeed do not differ by more than 0.1%, and thus the slant columns have been observed under almost identical viewing geometries. For these boxes, we take the standard deviation of the ensemble of slant-column as a reasonable estimate for the precision of the slant columns.

For 7 August 2006, we computed estimates for the slant column errors for every box between 60° S and 60° N. The results are shown in Fig. 5a for boxes with a relative difference between $\overline{V}$ and $\overline{V'}$ of less than 0.1%. The figure shows that there is no appreciable change of fitting error with latitude. Averaged over all latitudes, the fitting error is close to 0.75×10^{15} molec.cm^{-2} (dashed line). For the vertical column error, the contribution from the fitting error is smaller than 0.4×10^{15} molec.cm^{-2} (solid line, computed as σ_N/M_{tr}). We also made a distribution of all member deviations from box means and collected these deviations in a histogram (n=2893). This is shown in Fig. 5b. The distribution closely follows a Gaussian shape that is fitted to the histogram data. The fact that the distribution follows a Gaussian distribution is consistent with our assumption that the variability within each box is dominated by random errors in the slant columns, originating from measurement noise. The corresponding width of

the Gaussian for this day is 0.67×10^{15} molec.cm^{-2}, and we interpret this as a reasonable estimate for the average slant column error of all 2893 pixels we investigated on 7 August 2006. We also looked into a few other days and other longitude bands with different across-track variability corrections, and found very similar numbers. The slant column error for an individual OMI pixel is somewhat larger than the better-than-10% ($\approx0.3\times10^{15}$ molec.cm^{-2}) number quoted in Boersma et al. (2002). This number was computed from synthetic spectra (i.e. without across-track variability) under the assumption that 4 OMI pixels would be binned (increasing signal-to-noise by a factor of 2). For individual pixels, the OMI fitting error is larger than the 0.45×10^{15} molec.cm^{-2} found for GOME (Boersma et al., 2004) and SCIAMACHY (I. DeSmedt, personal communication), consistent with the higher signal-to-noise ratios for individual GOME and SCIAMACHY pixels than for OMI pixels.

5 Stratospheric contribution and tropospheric air mass factor

5.1 Stratospheric slant column

In order to determine the tropospheric NO_2 column accurately, the stratospheric component of the slant column density needs to be predicted. We attain this by data-assimilation of OMI slant columns in TM4:

- Modelled NO_2 profiles are convolved with the appropriate averaging kernel to give model-predicted slant column densities. The differences between observed and modelled columns (the model innovations) are used to force the modelled columns to generate an analysed state that is based on the modelled NO_2 distribution and the OMI observations.
- The forcing depends on weights (from observation representativeness and model errors) attributed to model and observation columns. Observed columns are attributed a low weight in regions and times with large tropospheric model columns.

This reflects the uncertainty in the averaging kernel, and minimizes the influence of slant columns with an estimated large tropospheric contribution.

– The forcing equation (based on the Kalman filter technique) is solved with the statistical interpolation method. This involves a covariance matrix that describes the forecast error and spatial correlations. The most important characteristics of this forecast covariance matrix are: (1) the conservation of modelled profile shapes. The altitude dependence of the forecast error is set to be proportional to the local NO_2 profile shape. (2) The horizontal correlation model function is assumed to follow a Gaussian shape with a $1/e$ correlation length of 600 km. This length was derived from the assimilation of ozone in the stratosphere (Eskes et al., 2003) and should be a reasonable guess for stratospheric NO_2 as well. (3) In addition we introduce a correlation scaling to reduce the correlation with increasing differences in concentration (Riishøjgaard, 1998). This avoids problems with negative concentrations near sharp gradients that occur for instance at the polar vortex edge. (4) The vertical distribution of the assimilation increments is determined by the covariance matrix and the averaging kernel profile. The kernel peaks in most cases in the stratosphere, which is an additional reason why the adjustment caused by the assimilation is mainly taking place in the stratosphere.

– The adjustments made by the assimilation are therefore mainly occurring in the stratosphere at places where the tropospheric concentrations are low. The stratospheric information inserted by the assimilation is transported to the stratosphere above more polluted areas by the advection in the model.

– The model NO_x species (NO, NO_2, NO_3, N_2O_5, HNO_4) are assumed to be fully correlated and are all scaled in the same way as NO_2.

– Based on the most recent analysed state, a forecast run of the model predicts the stratospheric field. This is used by the near-real time retrieval branch as shown in Fig. 2.

For further reading on the assimilation method we refer to Eskes et al. (2003). The advantage of the approach is that slant column variations due to stratospheric dynamics are now accounted for in the retrieval. The purpose is to improve the detection limit for tropospheric NO_2 columns that can be retrieved. An additional advantage is that the assimilation scheme provides a statistical estimate of the uncertainty in the stratospheric slant column. Generally, this statistical estimate is on the order of 0.1–0.2×10^{15} molec.cm^{-2}, much smaller than the slant column uncertainty reported on in the previous section. Hence, the detection limit in our method is mainly determined by the random slant column error (σ_S) that is easily averaged out by taking large numbers of observations. Not accounting for stratospheric dynamics however, would lead to systematic errors in the estimate of the stratospheric column (Boersma et al., 2004) that cannot be easily averaged out and would raise the detection treshold.

5.2 Tropospheric air mass factor

We convert the tropospheric slant column into a vertical column by using a tropospheric AMF (Eq. 1). For OMI NRT we follow as much as possible the same approach (same look-up tables, computational methods) as for the GOME and SCIAMACHY data set described in Sect. 3.1. But the forward model input parameters cloud fraction and cloud pressure differ between the OMI NRT and the GOME and SCIAMACHY RAM retrievals. This, along with the much finer spatial resolution of OMI compared to GOME, is expected to lead to different error budgets for OMI tropospheric NO_2 than for GOME and SCIAMACHY.

5.2.1 Cloud parameters

DOAS-type retrievals are very sensitive to errors in cloud parameters. Boersma et al. (2004) showed that errors in FRESCO cloud fractions of ±0.05 lead to retrieval errors of up to 30% for situations with strong NO_2 pollution. Errors in the cloud pressure may also affect retrievals, especially in situations where the retrieved cloud top is lo-

cated within a polluted layer. In such situations, errors in the cloud pressure of 50 hPa lead to retrieval errors of up to 25%.

Here we evaluate any differences between cloud parameters retrieved by SCIAMACHY and OMI. Cloud retrievals using FRESCO have been the subject of intensive validation. FRESCO applied on GOME measurements compared favourably to AVHRR (Koelemeijer et al., 2001) and ISCCP (Koelemeijer et al., 2002) cloud fractions (differences <0.02) and cloud pressure (differences <50–80 hPa). Of more relevance to our work is the application of FRESCO on SCIAMACHY measurements, as reported on by Fournier et al. (2006). They showed that FRESCO cloud parameters are in good agreement with other SCIAMACHY cloud algorithms, and estimate that the accuracy of the effective cloud fraction from FRESCO is better than 0.05 for all surfaces apart from snow and ice.

The retrieval methods for SCIAMACHY (FRESCO) and OMI (O_2–O_2) are based on the same principles, i.e. they both retrieve an effective cloud fraction, that holds for a cloud albedo of 0.8, and to do so, they both use the continuum top-of-atmosphere reflectance as a measure for the brightness, or cloudiness, of a scene. Furthermore they both use the depth of an oxygen band as a measure for the length of the average photon path from the Sun, through the atmosphere back to the satellite instrument. The length of this light path is converted to cloud pressure. On the other hand, there are some distinct differences between the cloud parameter retrievals from SCIAMACHY and OMI:

1. FRESCO uses reflectances measured inside and outside of the strong oxygen A band (758–766 nm), whereas the OMI cloud retrieval uses the weakly absorbing O_2–O_2 band at 477 nm.

2. FRESCO and O_2–O_2 have different sensitivities to cloud pressure. This originates from the use of absorption by a single molecule (FRESCO, O_2 A band), scaled with oxygen number density, versus the use of absorption by a collision complex (O_2–O_2), scaled with oxygen number density squared. This is expected to lead

to higher cloud pressures for the O_2-O_2 cloud algorithm.

3. SCIAMACHY observes clouds at 10:00 h local time, and OMI at 13:45 h local time.

Because SCIAMACHY and OMI observe the Earth at different times, FRESCO and O_2-O_2 cloud parameters cannot be compared directly. However, since temporal variation in global cloud fraction and cloud pressure between 10:00 h and 13:30 h is small (Bergman and Salby, 1996), frequency distributions of cloud parameters may be compared as a first evaluation of consistency between the two cloud retrievals. Here we compare SCIAMACHY FRESCO cloud retrievals version SC-v4 (August 2006, with improved desert surface albedos) to OMI O_2-O_2 retrievals v1.0.1.1 (available since 7 October 2005, orbit 6541). We compare the cloud retrievals for locations between 60° N and 60° S to avoid situations with ice and snow, where cloud retrieval traditionally is difficult. We gridded FRESCO and O_2-O_2 cloud parameters to a common 0.5°×0.5°grid and selected only grid cells filled with successfully retrieved cloud values for both FRESCO and O_2-O_2. Doing so, we obtain SCIAMACHY and OMI cloud parameter distributions on a spatial grid comparable to the SCIAMACHY grid ($30\times60\,km^2$) that have been sampled on the same days and locations.

Figure 6a shows the cloud fraction distribution as observed by FRESCO (dashed line) and O_2-O_2 averaged over the period 5–11 August 2006. The distributions show a high degree of similarity, with the smallest effective cloud fractions observed most often. The differences between the two distributions are most appreciable for small effective cloud fractions, with OMI more frequently observing cloud fractions smaller than 0.05, and SCIAMACHY more frequently observing cloud fractions in the 0.05–0.20 range. These differences are likely related to different surface albedo data bases used in the cloud retrievals, and the way effective cloud fractions outside the 0.0–1.0 range are treated. The O_2-O_2 retrieval uses the TOMS/GOME surface albedo datasets at 463 and 494.5 nm, consistent with albedos used for NO_2 AMF computations. But for FRESCO, the GOME albedo dataset at 760 nm is used. Since OMI's horizontal resolution is much finer than the 1°×1°surface albedo datasets, this will lead

to cloud fraction errors, especially for small cloud fractions. On average for 5–11 August 2006, FRESCO observes a mean effective cloud fraction of 0.311, and O_2–O_2 observes 0.300. The small mean difference between FRESCO and O_2–O_2 of 0.011 is encouraging and gives a first order indication of the accuracy of the O_2–O_2 cloud fraction retrieval.

Because the FRESCO version SC-v4 (August 2006) does not account for Rayleigh scattering (reflectances at the top-of-atmosphere are modelled by a purely O_2-absorbing atmosphere), FRESCO cloud pressures are likely to be underestimated for small cloud fractions. This effect has been discussed by Wang et al. (2006) for GOME and they showed that taking into account Rayleigh scattering in the GOME FRESCO retrieval on average increases cloud pressures by 60 hPa (for cloud fractions larger than 0.1). To avoid the effects of neglecting Rayleigh scattering in our comparison of FRESCO (that does not account for Rayleigh scattering) and O_2–O_2 (that does account for Rayleigh scattering), we have restricted ourselves to situations with cloud fractions higher or equal to 0.05, where the signal from Rayleigh scattering is outshined by the signal from the cloudy part of the scene. Figure 6b shows the distributions of cloud pressures observed by FRESCO (dashed line) and O_2–O_2 averaged over the period 5–11 August 2006. The figure shows that O_2–O_2 more frequently retrieves high cloud pressures than FRESCO. On average, O_2–O_2 cloud pressures are 58 hPa higher than FRESCO cloud pressures. As discussed above, O_2–O_2 retrievals are more sensitive to levels deeper in the cloud, as the absorber slant column scales with the oxygen number density (or pressure) squared profile rather than with the single oxygen molecule number density profile as in the FRESCO retrieval. It is important for the NO_2 retrieval to use the most appropriate cloud pressure in the context of the AMF computation. The "best" cloud pressure is the pressure level that, within the concept of the Lambertian reflector, indicates the effective scattering height for photons (in the 405–465 nm range). Dedicated validation campaigns with simultaneous observations of NO_2 profiles and cloud parameters that coincide with OMI observations will help address these issues.

5.2.2 Profile shape and representativity issues

In previous work, we estimated that errors in the a priori profiles obtained from a 3-D CTM give rise to approximately 10% error in the retrieved NO_2 columns (Boersma et al., 2004). Since then, Martin et al. (2004) and Schaub et al. (2006) showed that vertical distributions of NO_2 over southern U.S. and over northern Switzerland calculated with a CTM (GEOS-Chem and TM4 respectively) are consistent with observed NO_2 profiles in these regions, increasing confidence in the model-derived a priori profile shapes.

For OMI (as well as for reprocessed GOME and SCIAMACHY data), a priori NO_2 profile shapes are obtained from TM4, the successor of TM3. In earlier retrievals, the a priori profile shape was sampled at the TM3 spatial resolution of $5^\circ \times 3.75^\circ$. TM4 vertical distributions are now sampled at $3^\circ \times 2^\circ$. This resolution is still too coarse to properly resolve vertical distributions at OMI-scale resolution (roughly $0.1^\circ \times 0.1^\circ$). Thus a certain degree of spatial smearing or smoothing may be expected. This also holds for the surface albedo (Koelemeijer et al., 2003; Herman and Celarier, 1997), stored on a $1.0^\circ \times 1.25^\circ$-grid. Sub-grid variation in albedo, for instance as a result of land-sea or land-snow transitions, will lead to smearing errors in the final retrieval product. One other source of error that may lead to significant retrieval errors for high spatial resolution instruments such as SCIAMACHY and OMI is surface pressure (or altitude). Retrieval algorithms that use surface pressures from a coarse-resolution CTM-run typically undersample surface pressure over regions with marked topography. For instance over northern Switzerland this leads to significant retrieval errors (Schaub et al., 2006b), suggesting that future retrievals need to use surface pressure fields at a resolution compatible with the satellite observations.

5.2.3 Error budget

Table 1 compares contributions to AMF errors for polluted situations as presented in Boersma et al. (2004) for GOME to our best estimates for OMI in this work. We estimate that the uncertainty in the O_2–O_2 cloud fractions is ±0.05. Although the cloud

pressure uncertainty for OMI is comparable to that for GOME, there is a stronger sensitivity to cloud pressure errors for low clouds (OMI cloud pressures are on average 58 hPa higher than FRESCO coud pressures) within the polluted NO_2 layer (see Fig. 5b in Boersma et al., 2004). For GOME, with pixel sizes comparable to the grid size of the forward model input parameters (albedo, profile shape, surface pressure), undersampling errors could be discarded. But for OMI with its much smaller pixel size this can no longer be done. However, undersampling effects are relevant for some regions and times only. For instance, coarse-gridded surface pressures and albedos over a flat, rather homogeneous area like northern Germany will have little effect on fine-scale OMI retrievals. Over that same area though, spatial gradients in NO_2 profiles are not resolved by the 3° by 2° TM4 model, and this may lead to smearing errors. Since we have little quantitative information about undersampling errors, and because their effect is limited to certain locations and times (and highly variable), we indicate them in our table as ϵ_u (unknown undersampling error). Table 1 shows that the AMF error budget for individual retrievals from well quantified error sources is similar: 29% for GOME and 31% for OMI. However, previously discarded undersampling, or representativity errors, may contribute considerably to especially OMI AMF errors for specific locations and times. Again, these issues may be addressed through dedicated validation efforts and retrieval improvements including the use of high(er)-resolution surface pressure and albedo data bases, and improved spatial resolution chemistry-transport models.

Table 2 summarizes the contribution of various errors to the overall error budget for individual retrievals in cloud-free situations. Pixels are defined as cloud-free when the cloud radiance fraction does not exceed 50%, which corresponds to effective cloud fractions smaller than 15–20%. For comparison, in Table 2 we also included error estimates for GOME and SCIAMACHY retrievals computed with the RAM-approach. The uncertainty in the AMF is determined by errors in the forward model parameters as shown in Table 1. These error contributions are quite similar as in Boersma et al. (2004), although we expect that in certain locations and times smearing effects are larger for OMI than for SCIAMACHY and especially GOME. We estimate that a rough

1-sigma uncertainty for an individual OMI retrieval can be expressed as a base component (from spectral fitting uncertainty divided by AMF value, see Eq. 5 in Boersma et al., 2004) plus a relative uncertainty in the 10%–40% range due to AMF uncertainty. The base component is in the 0.5–1.5×10^{15} molec.cm^{-2} range (0.5×10^{15} molec.cm^{-2} for situations with high tropospheric AMF values, 1.5×10^{15} molec.cm^{-2} for situations with low tropospheric AMF values).

6 Intercomparison of OMI and SCIAMACHY tropospheric NO_2

We evaluate the consistency of OMI and SCIAMACHY tropospheric NO_2 retrievals for August 2006. The SCIAMACHY set has been retrieved with the RAM-approach, and has been described and validated in Blond et al. (2006)[1] and van der A et al. (2006). For all days on which both SCIAMACHY and OMI reported a cloud-free observation in the same 0.5°×0.5°grid cell, we averaged the data. Doing so, we avoid artificial differences that would otherwise show up as a consequence of the differences in spatial and day-to-day sampling between the two satellite instruments. As in the cloud parameter comparison, we have averaged the satellite data on a 0.5°×0.5°grid, as the size of these grid cells is in the same range as the size of an individual SCIAMACHY pixel (30×60 km^2). One important sampling difference remains as SCIAMACHY observations have been taken at 10:00 hr local time whereas OMI observations have been taken at 13:45 h local time.

Figure 7 shows the monthly mean tropospheric NO_2 field derived from SCIAMACHY and OMI for August 2006. For grey grid cells, the requirement that both SCIAMACHY and OMI have observed at least one, cloud-free scene in August 2006 has not been fulfilled. The spatial distributions tropospheric NO_2 observed by SCIAMACHY and OMI look consistent. Both satellite instruments observe the highest values over the industrial regions of North America, Europe, and China, and moderate levels of pollution in the biomass burning regions of South America, Southern Africa, and Northern Australia. Also, weak plumes of NO_2 over tropical oceans originating from especially

biomass burning and lightning in Africa, South America, and Australia, are observed by both SCIAMACHY and OMI.

The OMI mean tropospheric NO_2 field is much smoother than the SCIAMACHY field. This can be understood from the fact that 10× more pixels have been used in the OMI composite than in the SCIAMACHY composite, leading to much better statistics for the OMI average. Figure 7b also shows that after averaging the data over a month, features related to across-track variability may still be visible.

SCIAMACHY and OMI tropospheric NO_2 show appreciable consistency (r=0.77, n=1.9×10^5). For clean, unpolluted regions that make up the bulk of the grid cells, Fig. 7 shows quantitative agreement between OMI and SCIAMACHY. However, for strongly polluted regions, SCIAMACHY observes up to 30% higher values than OMI. We expect that these differences are to considerable extent due to differences in emissions, meteorological (boundary layer mixing, transport) and (photo) chemical regimes between 10:00 h and 13:45 h. Furthermore, we observe a strong land-sea contrast in tropospheric NO_2, especially over the Mediterranean. A manuscript with a detailed investigation of these differences is in preparation.

As a further illustration of OMI's capabilities, we show monthly averaged tropospheric NO_2 columns over Europe. Other than in Fig. 7, here we did not sample SCIAMACHY and OMI identically in space and time. We computed monthly averages on a 0.1°×0.1°grid to emphasize OMI's spatial resolution and sampled whenever a cloud-free observation was available. Figure 8 shows monthly mean tropospheric NO_2 columns from OMI (left panel) and from SCIAMACHY (right panel) in August 2006, a month with almost permanent cloud-cover over north-western Europe. The left panel shows that it was still possible to compute a monthly mean based on cloud-free OMI measurements. But SCIAMACHY – with less spatial and temporal coverage – did not record any cloud-free measurements over large parts of Europe, so that many grid cells show up grey in Fig. 8b. Apart from the better spatial and temporal coverage, the OMI average also shows much more spatial detail in the tropospheric NO_2 field. For instance, individual large cities including Madrid, Paris, and Moscow can be tracked

ACPD
6, 12301–12345, 2006

down easily on the OMI map. Industrial regions such as the Po Valley, the Ruhr Area, and large parts of the UK also stand out.

7 Conclusions

The DOMINO near-real time algorithm retrieves tropospheric NO_2 columns from OMI within 3 h after measurement. This is possible with a new technique that is based on the assimilation of recently observed OMI NO_2 slant columns in the TM4 CTM. After the most recent observations have been digested by the assimilation scheme, TM4 is run forward in time with forecast ECMWF meteorological fields to predict the required retrieval inputs. Because of this, these inputs (stratospheric slant column, NO_2 and temperature profile) are available when a newly processed orbit of NO_2 and cloud data arrives at KNMI, and retrieval of tropospheric NO_2 columns is completed within a few minutes upon arrival of the data. We introduced a correction method for across-track variability associated with calibration errors in the OMI level 1b data and show that our procedure removes most of the spurious across-track variability. A simple statistical approach has been used to estimate the uncertainty in the slant columns. We find that the random error in the slant column is approximately 0.70×10^{15}molec.cm^{-2} for a single OMI observation.

From a comparison of SCIAMACHY cloud parameters retrieved by FRESCO from the O_2 A band, and OMI cloud parameters retrieved from the O_2–O_2 absorption band at 477 nm, we find similar distributions of cloud fractions and cloud pressures. On average, SCIAMACHY cloud fractions are higher by 0.011 than OMI cloud fractions. OMI cloud pressures are approximately 60 hPa higher than FRESCO cloud pressures, consistent with different sensitivities of the two algorithms. The consistency between the SCIAMACHY and OMI cloud parameters, and the similar design and inputs for the NO_2 algorithms provide confidence in the OMI retrieval approach.

As a first-order test of OMI NRT NO_2 retrievals, we compared SCIAMACHY and OMI tropospheric NO_2 columns – identically sampled – for the month August 2006.

ACPD
6, 12301–12345, 2006

After regridding to a common 0.5°×0.5° grid, the only sampling difference is due to the 10:00 h SCIAMACHY and the OMI 13:45 h equator crossing time. The comparison shows that the two instruments observe the same spatial NO_2 patterns over the globe (r=0.77, n=1.9×10^5). The quantitative agreement between SCIAMACHY and OMI is appreciable over areas with little NO_2 pollution. Over polluted areas, OMI observes up to 30% smaller tropospheric NO_2 amounts than SCIAMACHY, related to differences in emissions, meteorology (boundary layer mixing, transport), and (photo) chemistry between 10:00 h and 13:45 h. This issue will be further investigated in a future study. Monthly mean maps of Europe, the U.S., and eastern Asia show the distribution of NO_2 with a large amount of detail.

We expect that for NO_2 from OMI, in contrast with the previous error analyses for GOME, a new type of retrieval error becomes increasingly relevant. Forward model parameters, including a priori profile shapes, surface albedo's, and surface pressures, are currently obtained from data bases with spatial resolutions much coarser than the actual spatial resolution of the retrieval. This is expected to lead to significant retrieval errors for some locations and times. We recommend detailed studies into the extent of these errors, and furthermore strongly encourage validation activities. Higher spatial resolution a priori information and models are needed for the full exploitation of the high resolution OMI data.

Acknowledgements. The near-real time retrieval was developed within the DOMINO project, "Derivation of Ozone Monitoring Instrument tropospheric NO_2 in near-real time", funded by the NIVR and the Dutch User Support Programme, project code USP 4.2 DE-31. The authors would like to thank D. Schaub (EMPA) and J. de Haan for useful discussions. Thanks to the NASA SIPS for processing the slant column near-real time NO_2 and cloud data, and delivery to the KNMI system. I. DeSmedt and M. Van Roozendael (BIRA) are kindly acknowledged for their retrievals of SCIAMACHY NO_2 slant columns.

References

Acarreta, J. R., De Haan, J. F., and Stammes, P.: Cloud pressure retrieval using the O_2–O_2 absorption band at 477 nm, J. Geophys. Res., 109, D05204, doi:10.1029/2003JD003915. 12308, 12311, 12312

Acarreta, J. R. and Stammes, P.: Calibration comparison between SCIAMACHY and MERIS on board ENVISAT, IEEE Geoscience and Remote Sensing Letters (GRSL), 2, 31–35, doi:10.1109/LGRS.2004.838348, 2005.

Beirle, S., Platt, U., Wenig, M., and Wagner, T.: Weekly cycle of NO_2 by GOME measurements: A signature of anthropogenic sources, Atmos. Chem. Phys., 3, 2225–2232, 2003. 12303

Beirle, S., Platt, U., Wenig, M., and Wagner, T. : NO_x production by lightning estimated with GOME, Adv. Space Res., 34, 793–797, 2004. 12303

Beirle, S., Spichtinger, N., Stohl, A., Cummins, K. L., Turner, T., Boccippio, D., Cooper, O. R., Wenig, M., Grzegorski, M., Platt, U., and Wagner, T.: Estimating the NOx produced by lightning from GOME and NLDN data: a case study in the Gulf of Mexico, Atmos. Chem. Phys. Discuss., 5, 11 295–11 329, 2005. 12303

Bergman, J. W. and Salby, M. L.: Diurnal Variations of Cloud Cover and Their Relationship to Climatological Conditions, J. Climate, 9, 2802–2820, 1996. 12321

Boersma, K. F., Bucsela, E. J., Brinksma, E. J., and Gleason, J. F.: NO_2, in: OMI Algorithm Theoretical Basis Document, vol. 4, OMI Trace Gas Algorithms, ATB-OMI-04, Version 2.0, edited by: Chance, K., pp. 13–36, NASA Distrib. Active Archive Cent., Greenbelt, Md., Aug. 2002. 12309, 12313, 12314, 12317

Boersma, K. F., Eskes, H. J., and Brinksma, E. J.: Error analysis for tropospheric NO_2 retrieval from space, J. Geophys. Res., 109, doi:10.1029/2003JD003962, 2004. 12304, 12309, 12312, 12317, 12319, 12323, 12324, 12325, 12335, 12336

Boersma, K. F., Eskes, H. J., Meijer, E. W., and Kelder, H. M.: Estimates of lightning NO_x production from GOME satellite observations, Atmos. Phys. Chem., 5, 2311–2331, 2005. 12303, 12310

Bogumil, K., Orphal, J., Homann, T., Voigt, S., Spietz, P., Fleischmann, O. C., Vogel, A., Hartmann, M., Bovensmann, H., Frerick, J., and Burrows, J. P.: Measurements of molecular absorption spectra with the SCIAMACHY Pre-Flight Model: instrument characterization and reference data for atmospheric remote-sensing in the 230–2380 nm region, J. Photoch. Photobio. A: Chemistry, 157, 167–184, 2003.

Bovensmann, H., Burrows, J. P., Buchwitz, M., Frerick, J., Nöel, S., Rozanov, V. V., Chance, K. V., and Goede, A. P. H., SCIAMACHY: Mission Objectives and Measurement Modes, J. Atmos. Sci., 56(2), 127–150, 1999. 12313

Bregman, A., Segers, A. J., Krol, M., Meijer, E. W., and Van Velthoven,P. F.: On the use of mass-conserving wind fields in chemistry-transport models, Atmos. Chem. Phys., 2, 447–457, 2003. 12311

Bucsela, E. J., Celarier, E. A., Wenig, M. O., Gleason, J. F., Veefkind, J. P., Boersma, K. F., and Brinksma, E. J.: Algorithm for NO_2 vertical column retrieval from the Ozone Monitoring Instrument, IEEE trans. on Geosci. Rem. Sens., 44, no. 5, doi:10.1109/TGRS.2005.863715. 12305, 12309, 12314, 12336

Cede, A., Herman, J., Richter, A., Krotkov, N., and Burrows, J.: Measurements of nitrogen dioxide total column amounts using a Brewer double spectrophotometer in direct sun mode, J. Geophys. Res., 111, D05304, doi:10.1029/2005JD006585, 2006. 12303

Dentener, F., Peters, W., Krol, M., van Weele, M., Bergamaschi, P., and Lelieveld, J.: Interannual variability and trend of CH_4 lifetime as a measure of OH changes in the 1979-2003 period, J. Geophys. Res., 108(D15), 4442, doi:10.1029/2002JD002916, 2003.

Dobber, M., Dirksen, R., Voors, R., Mount, G. H., and Levelt, P.: Ground-based zenith sky abundances and in situ gas cross sections for ozone and nitrogen dioxide with the Earth Observing System Aura Ozone Monitoring Instrument, Appl. Opt., 44(14), 2846–2856, 2005. 12307, 12314

Dobber, M., Dirksen, R., Levelt, P. F., van den Oord, G. H. J., Voors, R. H. M. et al.: Ozone Monitoring Instrument Calibration, IEEE T. Geosci. Remote., 44(5), 1209–1238, doi:10.1109/TGRS.2006.869987, 2006. 12307

Eskes, H. J and Boersma, K. F.: Averaging kernels for DOAS total-column satellite retrievals, Atmos. Chem. Phys., 3, 1285–1291, 2003. 12310

Eskes, H. J., van Velthoven, P. F. J., Valks, P., and Kelder, H. M.: Assimilation of GOME total ozone satellite observations in a three-dimensional tracer transport model, Q. J. R. Meteorol.Soc., 129, 1663, 2003. 12318, 12319

Fournier, N., Stammes, P., de Graaf, M., van der A, R., Piters, A., Grzegorski, M., and Kokhanovsky, A.: Improving cloud information over deserts from SCIAMACHY oxygen A-band measurements, Atmos. Chem. Phys., 6, 163–172, 2006. 12320

Heland, J., Schlager, H., Richter, A., and Burrows, J. P.: First comparison of tropospheric NO_2 column densities retrieved from GOME measurements and in situ aircraft profile measure-

ments, Geophys. Res. Lett. 29, 44, doi:10.1029/2002GL015528, 2002. 12303
Herman, J. R. and Celarier, E. A.: Earth surface reflectivity climatology at 340–380 nm from TOMS data, J. Geophys. Res., 102, 28 003–28 011, 1997. 12323
Houweling, S., Dentener, F. J., and Lelieveld, J.: The impact of nonmethane hydrocarbon compounds on tropospheric chemistry, J. Geophys. Res., 103, 10 673–10 696, 1998. 12311
Jaeglé, L., Martin, R. V., Chance, K. V., Steinberger, L., Kurosu, T. P. Jacob, D. J., Modi, A. I., Yoboué, V., Sigha-Nkamdjou, L., Galy-Lacaux, C.: Satellite mapping of rain-induced nitric oxide emissions from soils, J. Geophys. Res., 109, D21310, 10.1029/2004JD004787, 2004. 12303
Koelemeijer, R. B. A., Stammes, P., Hovenier, J. W., and de Haan, J. F.: A fast method for retrieval of cloud parameters using oxygen A-band measurements from the Global Ozone Monitoring Experiment, J. Geophys. Res., 106, 3475–3490, 2001. 12311, 12320
Koelemeijer, R. B. A., Stammes, P., Hovenier, J. W., and de Haan, J. F.: Global distributions of effective cloud fraction and cloud top derived from oxygen A band spectra measured by the Global Ozone Monitoring Experiment: Comparison to ISCCP data, J. Geophys. Res., 107(D12), 4151, doi:10.1029/2001JD000840, 2002. 12320
Koelemeijer, R. B. A., de Haan, J. F., and Stammes, P.: A database of spectral surface reflectivity in the range 335–772 nm derived from 5.5 years of GOME observations, J. Geophys. Res., 108 (D2), 4070, 10.1029/2002JD002429, 2003. 12312, 12323
Konovalov, I. B., Beekmann, M., Vautard, R., Burrows, J. P., Richter, A., Nüß, H., and Elansky, N.: Comparison and evaluation of modelled and GOME derived tropospheric NO_2 columns over Western and Eastern Europe, Atmos. Chem. Phys., 5, 169–190, 2005. 12303
Kurosu, T. P., K. Chance, and C. E. Sioris, Preliminary Results for HCHO and BrO from the Eos-Aura Ozone Monitorinhg Instrument, Proc. of SPIE, Vol. 5652, 116–123, 2005. 12314
Lauer, A., M. Dameris, A. Richter, and J. P. Burrows, Tropospheric NO_2 columns: a comparison between model and retrieved data from GOME measurements, Atmos. Chem. Phys., 2, 67–78, 2002. 12303
Leue, C., Wenig, M., Wagner, T., Klimm, O., Platt, U., and Jähne, B.: Quantitative analysis of NO_x emissions from GOME satellite image sequences, J. Geophys. Res., 106, 5493–5505, 2001. 12303
Levelt, P. F., van den Oord, G. H. J., Dobber, M. R., Mälkki, A., Visser, H. de Vries, J., Stammes, P., Lundell, J. O. V., and Saari, H.: The Ozone Monitoring Instrument, IEEE Trans. on Geosci. Rem. Sens., 44, no. 5, doi: 10.1109/TGRS.2006.872333, 2006(a). 12306

Levelt, P. F., Hilsenrath, E., Leppelmeier, G. W., van den Oord, G. H. J., Bhartia, P. K., Tamminen; J., de Haan, J. F., Veefkind, J. P., Science Objectives of the Ozone Monitoring Instrument, IEEE Trans. on Geosci. Rem. Sens., 44, 5, doi: 10.1109/TGRS.2006.872336, 2006(b). 12307

Ma, J., Richter, A., Burrows, J. P., Nüß, H., and van Aardenne, J. A.: Comparison of model-simulated tropospheric NO_2 over China with GOME-satellite data, Atmos. Environ., 40, 593–604, 2006. 12303

Martin, R. V., Jacob, D. J., Chance, K. V., Kurosu, T. P., Palmer, P. I., and Evans, M. J.: Global inventory of Nitrogen Dioxide Emissions Constrained by Space-based Observations of NO_2 Columns, J. Geophys. Res., 108, 4537, doi:10.1029/2003/JD003453, 2003. 12303

Martin, R. V., Parrish, D. D., Ryerson, T. B., Nicks, D. K., Jr., Chance, K., Kurosu, T. P., Jacob, D. J., Sturges, E. D., Fried, A., Wert, B. P.: Evaluation of GOME satellite measurements of tropospheric NO_2 and HCHO using regional data from aircraft campaigns in the southeastern United States, J. Geophys. Res., 109(D24), D24307, 10.1029/2004JD004869, 2004. 12303, 12323

Martin, R. V., Sioris, C. E., Chance, K., Ryerson, T. B., Bertram, T. H., Wooldridge, P. J., Cohen, R. C., Neuman, J. A., Swanson, A., and Flocke, F. M.: Evaluation of space-based constraints on global nitrogen oxide emissions with regional aircraft measurements over and downwind of eastern North America, J. Geophys. Res., 111, D15308, doi:10.1029/2005JD006680, 2006. 12303

van Noije, T. P. C., Eskes, H. J., Dentener, F. J., Stevenson, D. S., Ellingsen, K., et al.: Multi-model ensemble simulations of tropospheric NO_2 compared with GOME retrievals for the year 2000, Atmos. Chem. Phys. Discuss., 6, 2965–3047, 2006. 12303

Olivier, J., Peters, J., Granier, C., Pétron, G., Müller, J-F., and Wallens, S.: Present and future surface emissions of atmospheric compounds, POET report #2, EU project EVK2-1999-00011, 2003. 12311

van den Oord, G. H. J., Rozemeijer, N. C., Schenkelaars, V., Levelt, P. F., Dobber, M. R., Voors, R. H. M., Claas, J., ter Linden, M., de Haan, C., van de Berg, T.: OMI Level 0 to 1b Processing and Operational Aspects, IEEE Trans. on Geosci. Rem. Sens., 44, 5, doi: 10.1109/TGRS.2006.872935, 2006. 12308

Ordóñez, C., Richter, A., Steinbacher, M., Zellweger, C., Nüß, H., Burrows, J. P., and Prévôt, A. S. H.: Comparison of 7 years of satellite-borne and ground-based tropospheric NO_2 measurements around Milan, Italy, J. Geophys. Res., 111, D05310, doi:10.1029/2005JD006305,

2006. 12303
Petritoli, A., Bonasoni, P., Giovanelli, G., et al.: : First comparison between ground-based and satellite-borne measurements of tropospheric nitrogen dioxide in the Po basin, J. Geophys. Res., 109, D15307, doi:10.1029/2004JD004547, 2004. 12303
Platt, U.: Differential Optical Absorption Spectroscopy(DOAS), in Air monitoring by Spectroscopic Techniques, edited by: Sigrist, M. W., Chemical Analysis, 127, 1994. 12309
Richter, A., Burrows, J. P., Nüß, H., Granier, C., and Niemeier, U.: Increase in tropospheric nitrogen dioxide over China observed from space, Nature, 437, 129–132, doi:10.1038/nature04092, 2005. 12303
Riishøjgaard, L. P.: A direct way of specifying flow-dependent background error correlations for meteorological analysis systems, Tellus A 50, 42–57, doi:10.1034/j.1600-0870.1998.00004.x, 1998. 12318
Savage, N. H., Law, K. S., Pyle, J. A., Richter, A., Nüß, H., Burrows, J. P.: Using GOME NO_2 satellite data to examine regional differences in TOMCAT model performance, Atmos. Chem. Phys., 4, 1895–1912, 2004. 12303
Schaub, D., Boersma, K. F., Kaiser, J. W., Weiss, A. K., Folini, D., Eskes, H. J. and Buchmann, B.: Comparison of GOME tropospheric NO_2 columns with NO_2 profiles deduced from ground-based in situ measurements, Atmos. Chem. Phys., 6, 3211–3229, 2006. 12303, 12310, 12323
Schaub, D., Brunner, D., Boersma, K. F., Folini, D., Keller, J., Buchmann, B., and Staehelin, J.: Space-borne tropospheric NO_2 above the Alpine region: evidences for systematic retrieval errors and effect of inaccurate pixel surface pressure, submitted to ESA-ENVISAT conference 2007. 12323
Stammes, P.: Spectral radiance modeling in the UV-Visible range, IRS2000: Current problems in atmospheric radiation, edited by: Smith, W. L. and Timofeyev, Y. J., 385–388, A. Deepak, Hampton, Va, USA. 12311
Vandaele, A. C., Hermans, C., Simon, P. C., Carleer, M., Colin, R. S., Fally, M. F. Merienne, Jenouvrier, A., and Cocquart, B.: Measurements of the NO_2 absorption cross-section from 42 000 cm-1 to 10 000 cm-1 (238–1000 nm) at 220 K and 294 K, J. Quant. Spectrosc. Radiat. Transfer, 59, 171–184, 1998. 12314
van der A, R. J., Peters, D. H. M. U., Eskes, H. J., Boersma, K. F., Van Roozendael, M., De Smedt, I., and Kelder, H. M.: Detection of the trend and seasonal variation in tropospheric NO_2 over China, accepted, J. Geophys. Res., 111, D12317, doi:10.1029/2005JD006594,

2006. 12303, 12304, 12310, 12325
Veefkind, J. P. and de Haan, J. F.: DOAS total O_3 algorithm, in OMI Algorithm Theoretical Basis Document, vol. 2, OMI Ozone Product, ATB-OMI-02, Version 2.0, edited by: Bhartia, P. K., NASA Distrib. Active Archive Cent., Greenbelt, Md., Aug., 2002. 12308
Veihelmann, B. and Kleipool, Q.: Reducing Along-Track Stripes in OMI-Level 2 Products, TN-OMIE-KNMI-785, 2006.
Velders, G. J. M., Granier, C., Portmann, R. W., Pfeilsticker, K., Wenig, M., Wagner, T., Platt, U., Richter, A., and Burrows, J. P.: Global tropospheric NO_2 column distributions: Comparing 3-D model calculations with GOME measurements, J. Geophys. Res., 106, 12 643–12 660, 2001. 12303
Voors, R., Dobber, M., Dirksen, R., and Levelt, P.: Method of calibration to correct for cloud-induced wavelength shifts in the Aura satellites Ozone Monitoring Instrument, Appl. Opt., 45, 15, 3652–3658, 2006. 12314
Wang, P., Stammes, P., and Fournier, N.: Test and first validation of FRESCO+, accepted by SPIE Proceedings, 2006. 12322
Wenig, M., Kühl, S., Beirle, S., Bucsela, E., Jähne, B., Platt, U., Gleason, J., and Wagner, T.: Retrieval and analysis of stratospheric NO_2 from GOME, J. Geophys. Res., 109, D04315, doi:10.1029/2003JD003652, 2004.
WMO, Annual Report, Bass, Johnsten, 1975. 12314

Table 1. Overview of forward model error contributions to the (relative) AMF uncertainty for GOME and OMI. ϵ_{u_a} is the unknown error due to albedo undersampling, ϵ_{u_p} due to profile shape undersampling, and ϵ_U the overall undersampling AMF error that is highly variable in space and time.

Error source	GOME (Boersma et al., 2004) Uncertainty	GOME (Boersma et al., 2004) Uncertainty M_{tr}	OMI (this work) Uncertainty	OMI (this work) Uncertainty M_{tr}
Surface albedo	0.02	15%	0.02+ϵ_{u_a}	15%+ϵ_{u_a}
Cloud fraction	0.05	30%	0.05	30%
Cloud pressure	50–80 hPa	2%	60 hPa	15%
Profile shape	N.A.	9%	N.A.	9%+ϵ_{u_p}
Total AMF error		29%		31%+ϵ_U

Table 2. Contributions to the overall OMI tropospheric NO_2 retrieval error for individual, cloud-free pixels retrieved with the KNMI retrieval-assimilation-modelling approach (with the exception of the OMI standard product).
*It is anticipated that improved lv1 calibration (due Spring 2007) and standard-product correction for spurious across-track variability will reduce the OMI standard product NO_2 slant column uncertainty.
**For "mostly clear" conditions, Bucsela (personal communication, 2006) estimates 15–30% AMF uncertainty range.

Instrument	Reference	σ_S	$\sigma_{S_{st}}$	$\sigma_{M_{tr}}$
OMI near-real time product	This work	0.70×10^{15} molec.cm^{-2}	0.15×10^{15} molec.cm^{-2}	10%–40%
OMI standard product	Bucsela et al. (2006)	1.10×10^{15}* molec.cm^{-2}	0.20×10^{15} molec.cm^{-2}	not given**
SCIAMACHY	Blond et al. (2006)[1], DeSmedt (2006)	0.47×10^{15} molec.cm^{-2}	0.25×10^{15} molec.cm^{-2}	10%–40%
GOME	Boersma et al. (2004)	0.45×10^{15} molec.cm^{-2}	0.25×10^{15} molec.cm^{-2}	15%–50%

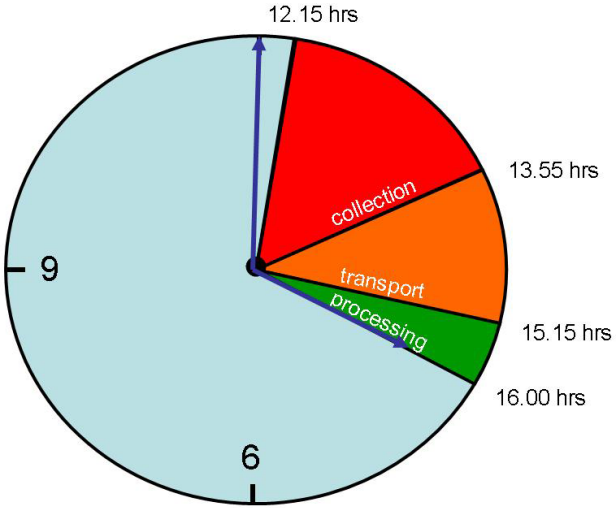

Fig. 1. OMI science data is linked down to ground stations once per orbit, resulting in a time delay between the OMI observations and reception at the ground station of at most 100 min. The collection, time-ordering, consecutive transfers, and level 1b and 2 processing, takes approximately 80 min. Final processing, image generation and web publishing generally occurs within 45 min.

ACPD
6, 12301–12345, 2006

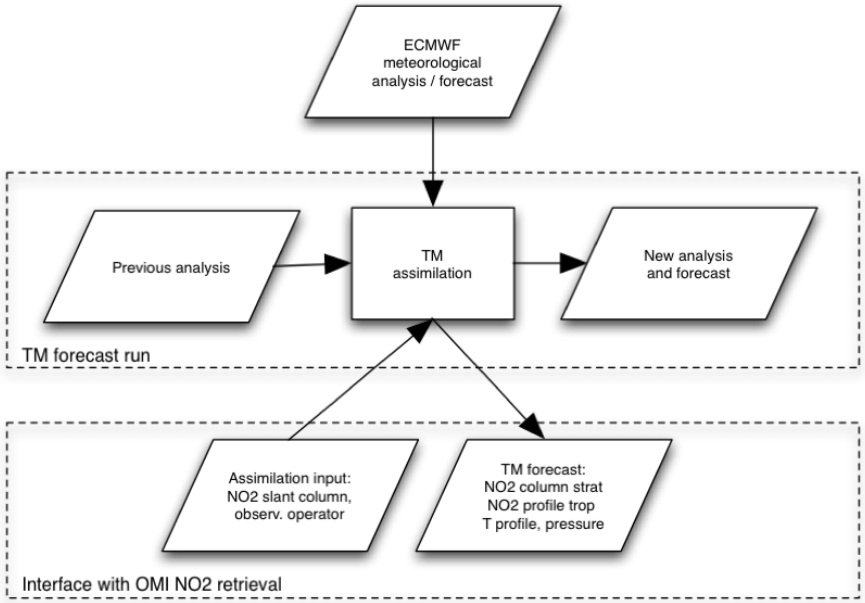

Fig. 2. Flowchart for the DOMINO forecast/assimilation subsystem. The lowest part shows the input-output interface with the NRT-subsystem.

ACPD
6, 12301–12345, 2006

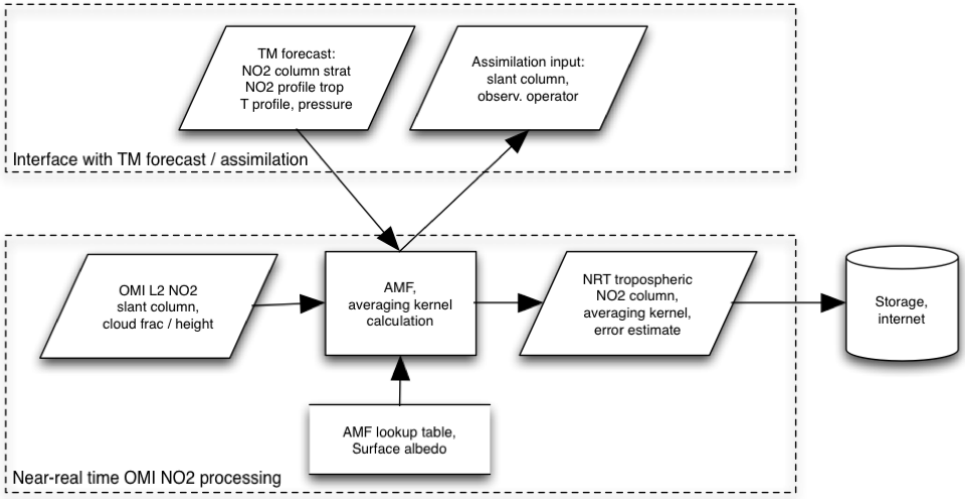

Fig. 3. Flowchart for the DOMINO NRT-subsystem. The upper part shows the input-output interface with the forecast/assimilation-subsystem (the lower part of Fig. 2).

ACPD
6, 12301–12345, 2006

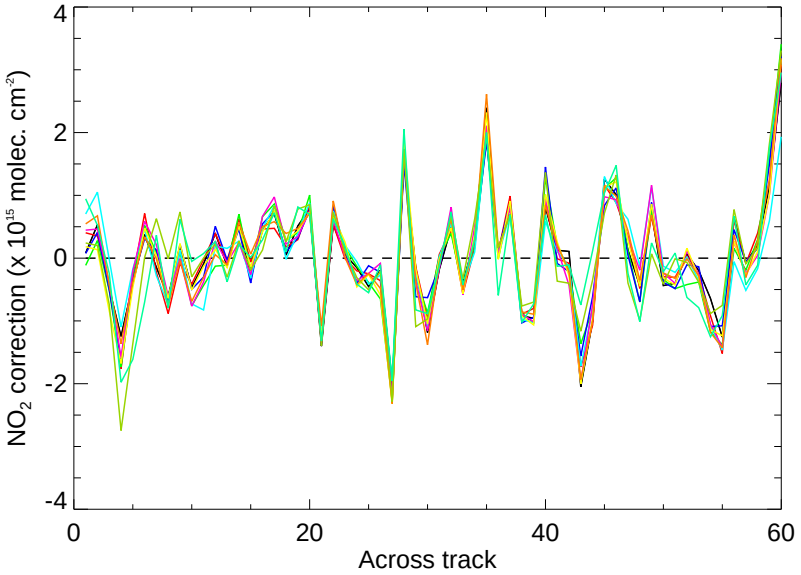

Fig. 4. Across-track variability corrections, computed with the method described in Sect. 4.1, for 10 consecutive orbits on 22 September 2004. Every orbital correction is shown with a unique colour.

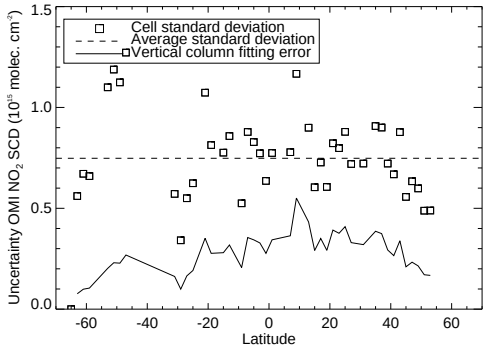

Fig. 5. **(a)** Left panel: standard deviation of slant columns within a 2°×2°(longitudes between 178° and 180° W) box as a function of latitude. The dashed line shows the meridional average of the standard deviations for all the boxes. The solid line shows the contribution of the (slant column) fitting error to the vertical column error (i.e. S/M_{tr}). **(b)** Right panel: distribution of member deviations from box means for 2893 pixels. The dashed line shows a Gaussian function fitted to the histogram data. The width of the Gaussian corresponds to a slant column error of 0.67×10^{15} molec.cm^{-2}.

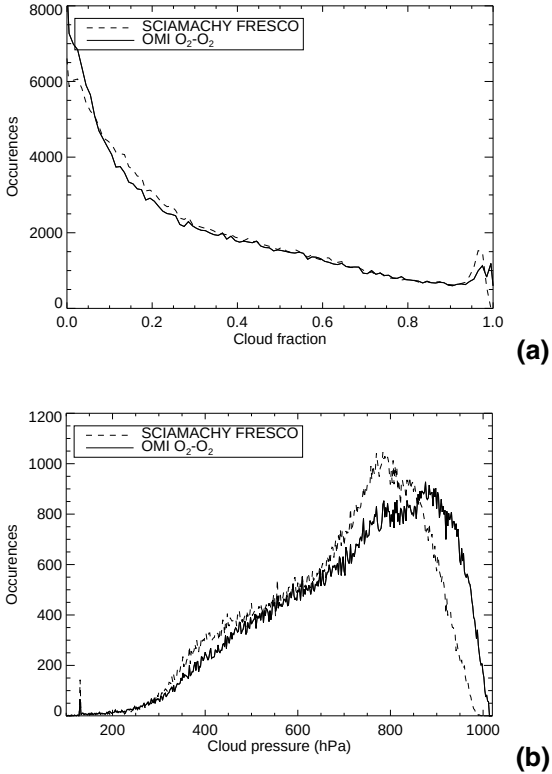

Fig. 6. **(a)** Left panel: histogram of 0.5°×0.5° gridded effective cloud fractions from SCIAMACHY FRESCO (dashed line) and OMI O_2-O_2 for seven consecutive days (5–11 August 2006). **(b)** Right panel: histogram of 0.5°×0.5° gridded effective cloud pressures from SCIAMACHY FRESCO (dashed line) and OMI O_2-O_2 for seven consecutive days (5–11 August 2006). Only observations with a cloud fraction higher or equal to 0.05 are shown.

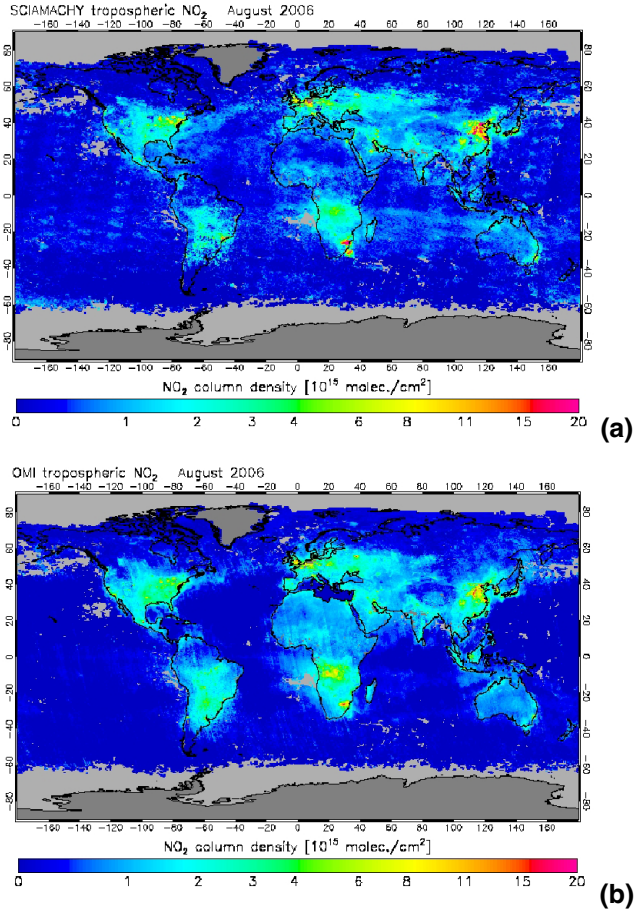

Fig. 7. (a) Monthly mean tropospheric NO_2 column from SCIAMACHY for situations when both SCIAMACHY and OMI observed a cloud-free scene. Grey grid cells have not been observed or had persistent cloud cover over August 2006. **(b)** Same as (a), but now for OMI.

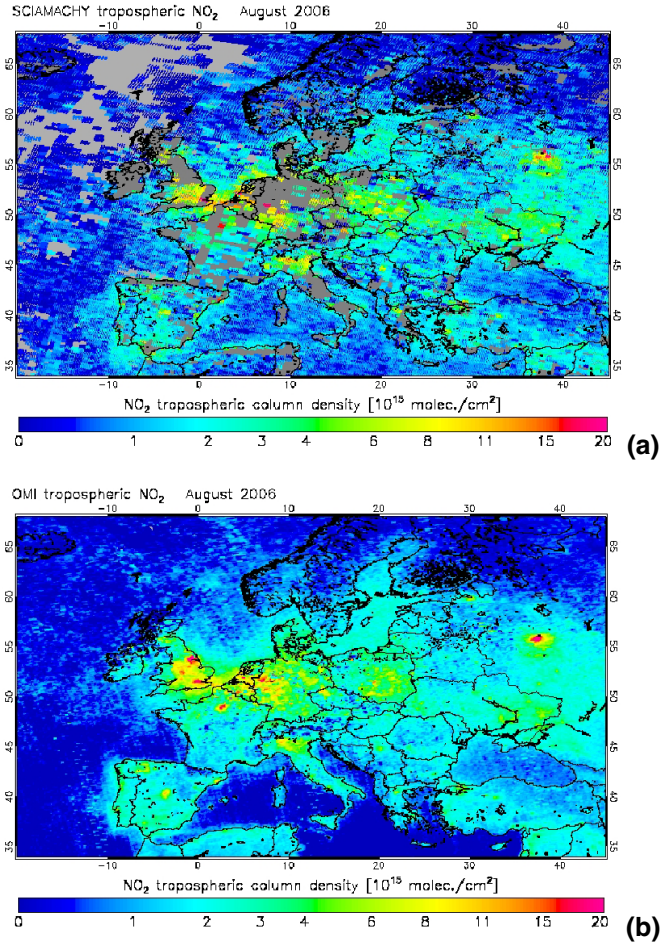

Fig. 8. (a) Monthly mean tropospheric NO_2 column from SCIAMACHY (left panel) for cloud-free situations. Grey grid cells have not been observed or had persistent cloud cover over August 2006. **(b)** Same as (a), but now for OMI.

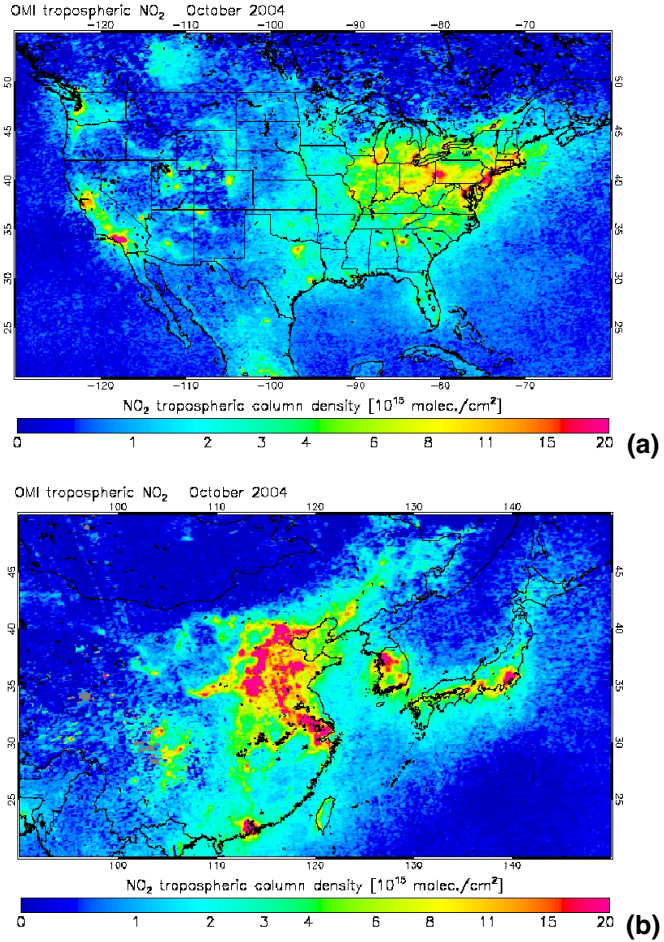

Fig. 9. **(a)** Monthly mean tropospheric NO_2 column from OMI over the U.S. for cloud-free situations. Grey grid cells have not been observed or had persistent cloud cover over October 2004. **(b)** Same as (a), but now over eastern Asia.